Available online at www.sciencedirect.com
ScienceDirect
Biomaterials 29 (2008) 2477–2489
Biomaterials
www.elsevier.com/locate/biomaterials

Substrate architecture and fluid-induced shear stress during chondrocyte seeding: Role of α5β1 integrin

Caroline G. Spiteri [a,b], Edmond W.K. Young [b,c], Craig A. Simmons [b,c], Rita A. Kandel [a,b,*], Robert M. Pilliar [a,b]

[a] CIHR-BioEngineering of Skeletal Tissues Team, Mount Sinai Hospital, Toronto, ON, Canada
[b] Institute of Biomaterials and Biomedical Engineering, University of Toronto, Toronto, ON, Canada
[c] Department of Mechanical and Industrial Engineering, University of Toronto, Toronto, ON, Canada

Received 16 November 2007; accepted 13 January 2008
Available online 7 March 2008

Abstract

Chondrocyte behaviour has been shown previously to be influenced by the architecture of the substrate on which the cells are grown. Chondrocytes cultured on fully porous titanium alloy substrates showed greater spreading and more matrix accumulation when compared to cells grown on porous-coated substrates with solid bases. We hypothesized that these features developed because of differences in fluid-induced shear stresses due to substrate architecture and that integrins mediate these responses. Computational fluid dynamics analyses predicted that cells on fully porous substrates experience time-dependent shear stresses that differ from those experienced by cells on porous-coated substrates with solid bases where media flow-through is restricted. To validate this model, the seeding protocol was modulated to affect fluid flow and this affected cell spreading and matrix accumulation as predicted. Integrin blocking experiments revealed that α5β1 integrins regulated cell shape under these two conditions and when cell spreading was prevented the increased accumulation of collagen and proteoglycans by chondrocytes seeded on fully porous substrates did not occur. Identifying the substrate-induced mechanical and molecular mechanisms that influence chondrocyte behaviour and tissue formation may ultimately lead to the formation of a tissue that more closely resembles natural articular cartilage.

Keywords: Cartilage tissue engineering; Cell spreading; Computational fluid dynamics; Integrin; Titanium alloy

1. Introduction

Although bioengineering of articular cartilage is receiving considerable attention, the techniques utilized in the process have yet to be optimized. One approach by which the quality of this tissue may be enhanced is by altering the design of the substrate on which the cells are grown. In a previous study we observed differences in chondrocyte morphology and matrix accumulation on two nearly identical Ti-6Al-4V porous substrates. As the surfaces seen by the cells were identical, the only difference between these two substrates was that one contained a solid base to which the sintered porous structure was bonded (porous-coated) whereas the other substrate lacked this solid base [1]. We showed that chondrocyte spreading was greater on the fully porous substrate, and that these cells accumulated significantly more extracellular matrix than those grown on the porous-coated substrate. The mechanisms underlying these chondrocyte responses are not known.

A variety of molecules are responsible for cell attachment and spreading and of these integrins appear to be important [2,3]. Integrins are heterodimeric transmembrane glycoproteins consisting of α and β subunits [4]. They can interact with components of the cartilage extracellular matrix that leads to outside–inside cell activation. Upon engagement, integrins serve as a scaffold for the assembly of multiple

* Corresponding author. Department of Pathology and Laboratory Medicine, Mount Sinai Hospital, 600 University Avenue, Suite 6-500-11, Toronto, ON, Canada M5G 1X5. Tel.: +1 416 586 8516.
E-mail address: rkandel@mtsinai.on.ca (R.A. Kandel).

0142-9612/$ - see front matter © 2008 Elsevier Ltd. All rights reserved.
doi:10.1016/j.biomaterials.2008.01.018

proteins that initiate a signalling cascade which regulates cell behaviour and gene expression. Integrins are able to interact with cytoskeletal proteins in the cytoplasm and regulate cell shape. Chondrocytes express a variety of integrins such as α5β1 which interacts with fibronectin or αvβ3 which can bind to both vitronectin and osteopontin. Engagement of various integrins by their ligands has been implicated in regulating chondrocyte spreading and survival *in vitro* [5]. It is therefore possible that the differences in chondrocyte morphology on substrates with varying geometries are mediated by specific integrins. Furthermore, chondrocyte cell shape has also been shown to influence matrix accumulation [6].

It is not clear how the presence of a solid base may affect integrin engagement and cell spreading but it may be inducing changes in fluid dynamics within the porous structure during the initial stages of cell seeding. This could result in alterations in fluid-induced shear stresses acting on the cells, which can affect chondrocytes and even enhance matrix accumulation [7–9]. It has been shown that shear stress, even at magnitudes as low as 3 mPa can affect chondrocyte morphology [10]. Several studies have demonstrated that integrins are involved in mechanotransduction and altering gene and/or protein expression by chondrocytes [11–14]. Thus the hypothesis of this study is that the mechanism by which changes in substrate architecture alter chondrocyte matrix accumulation is through fluid-induced shear stresses, which influences integrin-mediated cell spreading. To address this hypothesis, the time-dependent shear stress profiles were estimated during cell seeding for the different substrate architectures using fluid mechanics modeling. The model predictions were then tested by altering the shear stress temporal profile and analyzing chondrocyte shape and matrix accumulation. Finally, the role of integrins in regulating these responses was evaluated.

2. Methods

2.1. Titanium alloy disk fabrication

Titanium alloy substrates were fabricated as described previously [15]. Briefly, porous-coated substrates were made by sintering a 2-mm thick layer of Ti-6Al-4V powder on top of a 4 mm diameter, 2 mm thick solid disk. The fully porous substrates (4 mm diameter × 2 mm thick disks) were made with the same Ti-6Al-4V powder under the same sintering conditions. These two substrates will be referred to as "porous-coated" and "fully porous", respectively. All disks were then cleaned, passivated in nitric acid, encased in plastic tubing (Bev-a-line), and sterilized by gamma irradiation (2.5 mRad).

2.2. Chondrocyte culture

Chondrocytes were harvested from metacarpal–phalangeal bovine articular cartilage by sequential enzymatic digestion as described previously [16]. Cartilage from several animals was pooled to obtain sufficient cells for an experiment. Under sterile conditions cartilage was harvested and digested sequentially with protease and collagenase. Isolated chondrocytes were then re-suspended in Ham's F12 media supplemented with 5% fetal bovine serum (FBS) at a concentration of 5000 cells/μl. Tubing-encased substrates were placed in 24 well culture dishes and 0.5 mL of 5% FBS supplemented Ham's F12 was added to each well around the tubing-encased substrate (stage 1 of seeding). Two minutes later, the cell suspension was added to the top surface of the titanium alloy substrates at a density of 1.2×10^6 cells/cm^2 (150,000 cells total) (stage 2 of seeding), and allowed to adhere to the surface for 2 h at 37 °C, at which point, 1.5 mL of 5% FBS in Ham's F12 was added to each well to submerge the substrates. The constructs were maintained in these media for 24 h at 37 °C.

2.3. Computational fluid modeling

Fluent 6.2 software (ANSYS, Inc., Canonsburg, PA, USA) was used to simulate fluid flow through the three-dimensional geometry that represented the interstitial structure of the Ti-6Al-4V porous substrate. The model geometry consisted of a unit cell of spheres organized in a body-centred cubic (BCC) arrangement. This was found to be an appropriate model because of its simplicity, and because the porosity of a BCC structure (32%) is similar to the actual porosity of substrates used in our experiments (35%).

2.4. Integrin blocking

To evaluate the role of integrins in this system, antibody reactive with β1 (clone 4B4), α5β1 (clone JBS5), or αvβ3 (clone LM 609) integrins (1:100 dilution in Ham's F12 supplemented with 5% FBS, Chemicon International Inc., Temecula, CA, USA) was added to cell suspensions (5000 cells/μl; 100 μl) and placed on a shaker at 4 °C for 1 h. Integrin α5β1 was shown in a previous study to influence chondrocyte attachment [17]. These antibodies are known to block function [17]. Fully porous substrates were placed in 24 well dishes and 0.5 mL of the antibody solution was added to each well around the substrate. The antibody-containing cell suspension was placed on top of the titanium alloy substrates at a density of 1.2×10^6 cells/cm^2 and allowed to adhere to the surface for 2 h at 37 °C. An additional 1.5 mL of antibody solution was then added to each well in order to fully submerge the substrates. The cells were maintained in this solution for the remaining 24 h after which the constructs were harvested. Each condition was performed in triplicate and repeated at least three times using cells from different calves.

2.5. Chondrocyte morphology

Cells cultured for 24 h were rinsed three times in phosphate-buffered saline (PBS), fixed in 4% paraformaldehyde for 10 min, and rinsed three times in PBS. Samples were then dehydrated in graded ethanol series up to 100%, critical point dried (Bal-Tec, Leichtenstein; CPD 030), and sputter-coated with gold (Denton Vacuum, Moorestown, NJ; Desk II). The cells were visualized by secondary electron imaging under scanning electron microscopy (FEI, Hillsboro, OR; XL30) to compare cell morphology and size on the various substrates under the various conditions.

2.6. Chondrocyte area

Scanning electron micrographs of chondrocytes on the substrate were imported into ImageJ, a public domain image-processing program available at http://rsb.info.nih.gov/ij/. The scale was set using the scale bar in the images. Chondrocyte area was determined by tracing the cell outline and calculating the area using the ImageJ program. Only cells that were in direct contact with the substrate were measured. Approximately 30 cells were measured per substrate, three substrates were used for each condition, and each experiment was repeated three times.

2.7. Collagen and proteoglycan accumulation

To determine the role of integrin(s) on the accumulation of newly synthesized collagen and proteoglycans, cultures were incubated with [^{35}S]–SO_4 (2 μCi/sample) and [^{3}H]-proline (2 μCi/sample) immediately following cell seeding. After 24 h, samples were harvested, separated from the tubing, and washed three times in PBS. The cells were then digested with papain for 48 h at 65 °C, and an aliquot of papain digest was counted in a β-liquid scintillation counter (Beckman Coulter, CA). The counts were normalized for the DNA content (an indication of cell number) on the substrate, which had been measured by fluorometric analysis, as described previously [18].

2.8. Statistical analysis

All experiments were repeated at least three times, results pooled, and expressed as the mean ± standard error of the mean. Results were analyzed using a one-way analysis of variance and all pair-wise comparisons between groups were conducted using the Tukey *post hoc* test. Significance was assigned at p-values less than 0.05.

3. Results

3.1. Computational fluid modeling

To estimate the magnitude of local shear stresses acting on the bead surfaces, we numerically simulated fluid flow through the porous substrates using a commercially available computational fluid dynamics package. Fig. 1A shows the geometry used in the simulations and results obtained for local interstitial fluid velocity u and bead surface shear stress τ_w (referred to as wall shear stress hereafter) at specific locations in the geometry. For quantitative analysis, Fig. 1B shows spatial variation of local interstitial fluid velocity along a vertical axis of symmetry between the spheres (white dashed line in Fig. 1A). The numerical results indicate that for an inlet average interstitial fluid velocity of $v_{if} = 1$ μm/s, the local interstitial fluid velocities can reach a maximum of $u = 3.88$ μm/s. For a BCC unit cell of height H ($H = 105$ μm in our simulations), these velocity maxima occur at $0.25H$ and $0.75H$ (graph indicates maxima occur at $H = 26$ μm and 78 μm for the bottom unit cell), which coincide with horizontal planes that slice through the BCC architecture at cross-sections with the least available pore area for fluid penetration. This is in agreement with the law of continuity.

Fig. 1C shows a plot of the local wall shear stress τ_w on the bead surface with respect to vertical position. The plot indicates that maximum local wall shear stress $\tau_w = 0.76$ mPa when $v_{if} = 1$ μm/s, and occurs close to the equator of the sphere. This would be expected as fluid motion devotes its contribution solely to shear stress near the equator, where the interstitial space is at a minimum [19]. In contrast, fluid motion divides its contribution between normal and tangential stress components at most other latitudes, thus lowering the local shear stress at these latitudes.

These numerical results were used in conjunction with theoretical analyses of the fluid flow time profiles for the fully porous and porous-coated substrates to estimate the time-dependent shear stress applied to the cells introduced into the system during stage 2 of seeding.

3.2. Analysis of fluid flow through porous substrates

Differences in the three-dimensional architectures of the two substrates resulted in distinct time-dependent fluid flow profiles through the pores of the structure. During stage 1, where 0.5 mL of supplemented media were added to the well outside of the tubing-encased substrate, fluid seeped in from the bottom and percolated upwards through the fully porous substrate. In 2 min just prior to cell seeding on this substrate, the fluid–air interfaces inside and outside the tubing equilibrated as a result of balancing hydrostatic and surface tension forces. This equilibrium of interfaces was in contrast to what occurred for the porous-coated substrate where fluid flow was blocked by the solid base, and thus, no upward percolation through the pores occurred. The porous section of the porous-coated substrate therefore remained dry until stage 2, when cell-containing media were added.

The difference in Ti-6Al-4V substrate architectures resulted in distinct fluid flow time profiles during stage 2 of the cell seeding procedure when the cell suspensions were loaded on top of their respective substrates. In the fully porous structure,

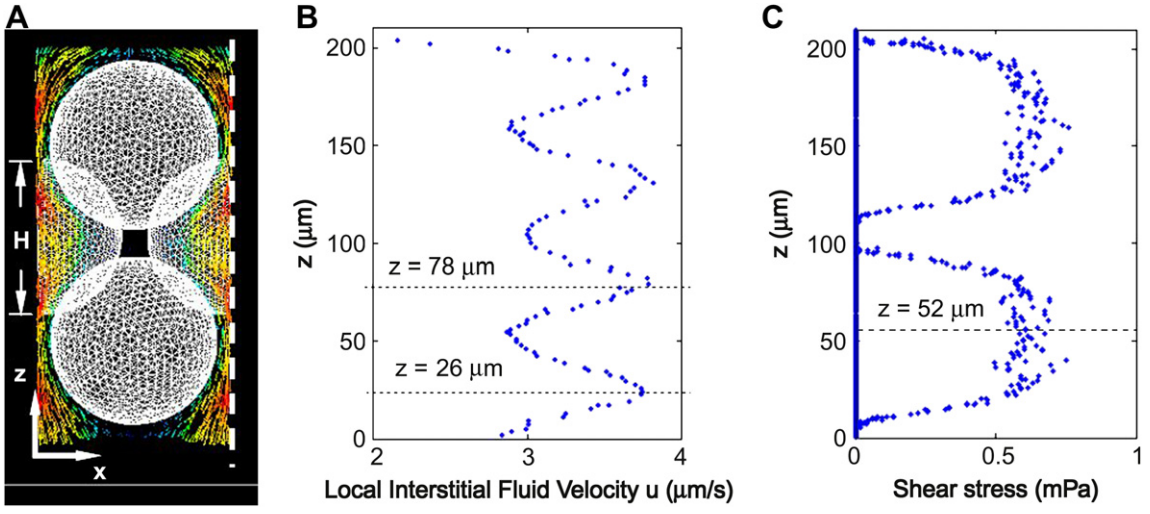

Fig. 1. Computational results for local interstitial fluid velocity and wall shear stress. (A) Three-dimensional mesh geometry of body-centred cubic (BCC) arrangement of spheres as model geometry for porous substrate architecture. Two whole spheres are shown with two spheres in the background. Other neighbouring spheres have been removed for clarity. Coloured velocity vectors indicate regions of high flow (red) and regions of low flow (green/blue). Dashed line represents a plane of symmetry. (B) Local velocity u with respect to vertical position z, for velocity along the white dashed line of (a). Peak local velocities within pores are 3.88 μm/s at $z = 26$ μm and $z = 78$ μm, for an inlet average interstitial fluid velocity $v_{if} = 1$ μm/s. (C) Local wall shear stress on the sphere surfaces with respect to z. Peak shear stress is 0.76 mPa for $v_{if} = 1$ μm/s, and occurs at the equator of a sphere ($z = 0.52$ μm).

the pores were already filled with the media added during stage 1 (see Fig. 2A). The addition of the cell suspension within the tubing channel led to an imbalance in interface levels and increase in hydrostatic pressure that induced pressure-driven flow through the porous bed and into the well. It can be shown analytically that this pressure-driven flow acts transiently, and that the average velocity of the cell suspension within the interstices of the porous bed, v_{if}, is governed by an exponential decay:

$$\text{Fully porous}: \; v_{if}(t) = \frac{k\rho g h_{cell}}{\phi \mu L} e^{-t/\tau}, \quad t \geq 0 \tag{1}$$

where τ is the time constant of the system, given by:

$$\tau = -\frac{\mu L}{k\rho g}\left(\frac{r_{iw}^2 - r_{ot}^2}{r_{iw}^2 - r_{ot}^2 + r_{it}^2}\right) \tag{2}$$

In Eqs. (1) and (2), k is the specific permeability of the porous structure, and is a function of the substrate porosity ϕ, ρ is the fluid density, g is the acceleration due to gravity, h_{cell} is the height of the fluid column of the added cell suspension, μ is the fluid dynamic viscosity, L is the thickness of the porous structure, r_{it} and r_{ot} are the inner and outer radii of the tubing, and r_{iw} is the inner radius of the culture well. Details of the derivation are included in the Appendix.

In our experiments, $r_{it} = 2$ mm, $r_{ot} = 2.5$ mm, $r_{iw} = 9$ mm, $L = 2$ mm, $\phi = 0.35$, $\rho = 1000$ kg/m^3 and $\mu = 0.7 \times 10^{-3}$ N s/m^2 for an aqueous solution of media at 37 °C. h_{cell} is calculated to be 2.4 mm for a 30-μL cell suspension. Finally, the specific permeability k for a titanium-based substrate can be approximated using an empirical relationship between k and ϕ for porous titanium [20]:

$$\log\left(\frac{k}{0.99 \times 10^{-15}}\right) = -5.26 + 4.65 \log\left(100\phi\right) \tag{3}$$

For $\phi = 0.35$, permeability is $k = 8.2 \times 10^{-14}$ m^2. Substituting these values into Eqs. (1) and (2) yields an initial interstitial fluid velocity of $v_{if}(t=0) = 3.9$ μm/s, and a time constant $\tau = 27.5$ min. While the value used for specific permeability was not experimentally verified for our porous substrates, the time constant is in a good agreement with our observation that 2 h of incubation is sufficient for the system to return to equilibrium ($4\tau = 1$ h 50 min, and relates to 98% exponential decay).

In contrast, for the porous-coated structure, the 30 μL cell suspension added to the top of the substrate immediately begins to flow into the pores at a velocity much higher than the initial velocity for the fully porous structure. This higher velocity is due to the absence of media inside the pores of the substrate at $t = 0$, which would tend to buffer the fluid motion (see Fig. 2B). The interstitial fluid velocity in this case varies in a time-dependent manner as the fluid percolates deeper into the substrate toward the bottom of the porous region. Once the fluid reaches the bottom of the porous region (i.e. the top of the solid base) at $t = t_b$, the fluid motion ceases instantaneously (interstitial fluid velocity = 0). As can be shown, v_{if} for the porous-coated case is governed by

$$\text{Porous-coated}: \; v_{if}(h) = \begin{cases} \dfrac{k\rho g(1-\phi)}{\mu\phi}\dfrac{(h-h_0)}{(h-h_{cell})} & 0 < t \leq t_b \\ 0 & t > t_b \end{cases} \tag{4}$$

v_{if} can be related to time t through the function $t(h)$:

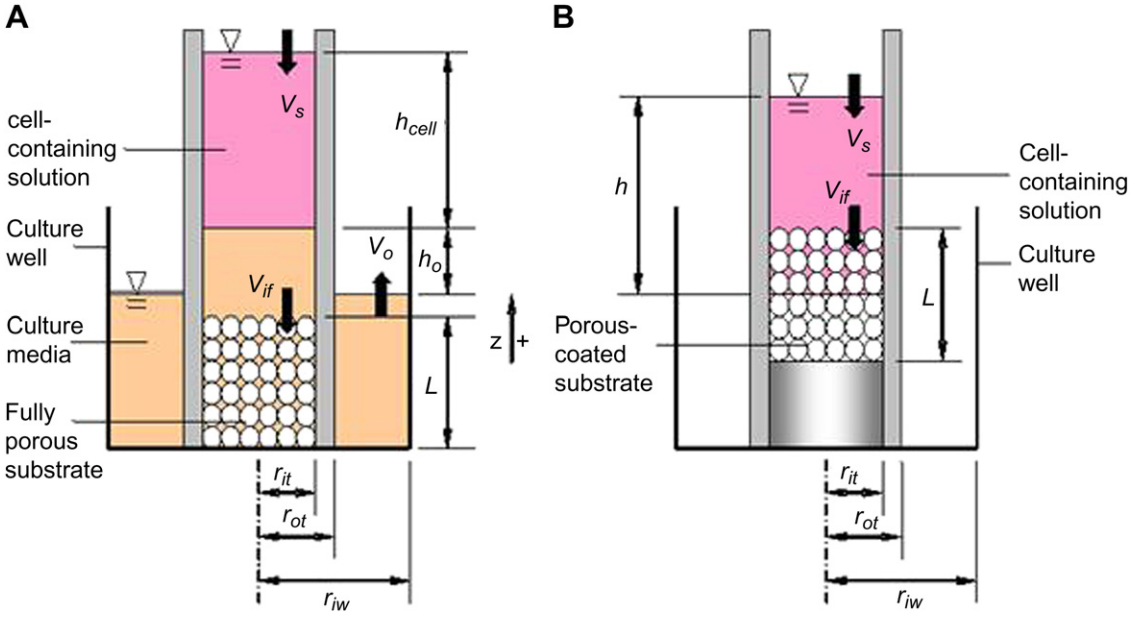

Fig. 2. (A) Fully porous substrate system just after cell seeding (beginning of stage 2) and (B) Porous-coated substrate system a short time after cell seeding (during stage 2). r_{it} is inner radius of cylinder; r_{ot} is outer radius of cylinder and tubing; r_{iw} is the radius of circular well; L is the thickness of the porous disk; h_0 is capillary height due to surface tension; h_{cell} is height of cell suspension added; h is time-dependent height of cell suspension (for porous-coated case); v_s is the superficial velocity; v_{if} is the interstitial fluid velocity; and v_o is the outflow velocity (in the well).

$$t(h) = \frac{\mu\phi}{k\rho g(1-\phi)^2}\left[(h-h_{\text{cell}}) + (h_0 - h_{\text{cell}})\ln\left(\frac{h-h_0}{h_{\text{cell}}-h_0}\right)\right] \quad (5)$$

Details of the derivation and discussion of the form of the equations are included in the Appendix. Using the same system parameters mentioned above, and recognizing that the total height of the fluid column at $t = t_b$ is $h_b = h_{\text{cell}} + (1-\phi)L$, we find through Eq. (5) that $t_b = 4.5$ min.

The relationships for the velocity of the cell-containing media with respect to time t are plotted in Fig. 3A. In addition, Fig. 3B shows complementary plots for maximum local shear stress versus time, which are identical to the interstitial fluid velocity curves except for a constant empirical factor K_0. Scaling arguments and the low Reynolds number assumption can be used to prove that $\tau_w = K_0 v_{if}$ for all time t. The numerical simulation results from above showed that $K_0 = 0.76$ mPa/(μm/s) since $\tau_w = 0.76$ mPa for $v_{if} = 1$ μm/s, and Fig. 3 reflects this similarity.

In the fully porous case, there is a gradual exponential decay of the maximum shear stress from $\tau_w = 3$ to $\tau_w = 0.3$ mPa in the first hour (based on time constant $\tau = 27.5$ min), so cells are constantly exposed to relatively low-shear stresses from the passing fluid after initial attachment. In contrast, for the porous-coated case, shear stress drops abruptly from $\tau_w > 10$ (not shown on axis) to $\tau_w = 3.4$ mPa in the first 4.5 min, and stops completely thereafter ($t > 4.5$ min). Thus, cells are not only initially exposed to much higher shear stress magnitudes, but shear stress gradients are also higher. Furthermore, cells are not exposed to a potentially beneficial mechanical stimulation due to shear stresses from low velocity fluid flow as was seen in the fully porous case.

3.3. Test of model predictions

In order to validate the model as well as test our hypothesis that shear stress profiles may regulate chondrocyte response, we designed a separate experiment combining separate portions of the time profiles. In this experiment, cells were seeded on a fully porous substrate, but stage 1 in the seeding protocol is eliminated such that no media initially resides within the pores to mimic the condition of the porous-coated substrate. As shown in Fig. 3, this third time profile combines the abrupt decrease in interstitial fluid velocity (and shear stress) in the initial 4.5 min with a gradual exponential decay. This time profile can be expressed mathematically as:

$$\text{Fully porous, no stage 1}: v_{if} = \begin{cases} \dfrac{k\rho g(1-\phi)}{\mu\phi}\dfrac{(h-h_0)}{(h-h_{\text{cell}})} & 0 < t \le t_b \\ \dfrac{k\rho g(h_{\text{cell}} - h_0 + (1-\phi)L)}{\phi\mu L}\, e^{-(t-t_b/\tau)} & t > t_b \end{cases} \quad (6)$$

Chondrocyte morphology and area on the fully porous substrate grown in the presence and absence of stage 1 in the seeding protocol were determined by scanning electron microscopy. While control chondrocytes (standard seeding protocol) had spread morphologies as expected, those cells that were grown in the absence of stage 1, appeared to be rounded, and displayed little evidence of spreading (Fig. 4A,B). This corresponded to a 40% decrease in cell area on average (Fig. 4C), which is comparable to the previously documented chondrocyte morphology on the porous-coated substrate [1].

As cell spreading correlated with increased matrix accumulation in our previous study, we examined whether the shear stress profile which appears to modulate cell shape will also alter matrix retention. The relative amounts of newly synthesized collagen and sulphated proteoglycan (normalized by DNA content) that accumulated by chondrocytes grown in the presence and absence of stage 1 on the fully porous Ti-6Al-4V substrates within the first 24 h of culture was quantified (Fig. 5). In the absence of stage 1, chondrocytes accumulated approximately 15% and 25% less collagen and proteoglycans, respectively, than cells seeded under standard conditions.

3.4. Role of integrins in mediating fluid-induced changes in chondrocyte behaviour

As these shear stresses influenced cell shape we postulated that the affect of these forces were transmitted via integrins. To evaluate which, if any, integrins were involved, chondrocytes were incubated in the presence and absence of function-blocking antibodies reactive with the β1 integrin subunit, the α5β1 integrin or the αvβ3 integrin. Blocking β1 as well as α5β1 integrin prevented chondrocyte spreading on the fully porous substrate (Fig. 6A,B). In contrast, cell spreading was not affected by incubation with the αvβ3 integrin antibody as the cell morphology and area were similar to the control cells.

To determine whether the changes in cell morphology correlated with an increase in matrix accumulation, chondrocyte synthesis of proteoglycans and collagen in the presence and absence of the β1 integrin blocking antibody were determined. In the presence of this antibody, both collagen and proteoglycan accumulation decreased by approximately 75% (Fig. 7).

4. Discussion

This study suggests that chondrocytes can experience shear forces during cell seeding that influence matrix accumulation. Computational fluid dynamic analyses predicted that cells on fully porous substrates experience different shear stress time

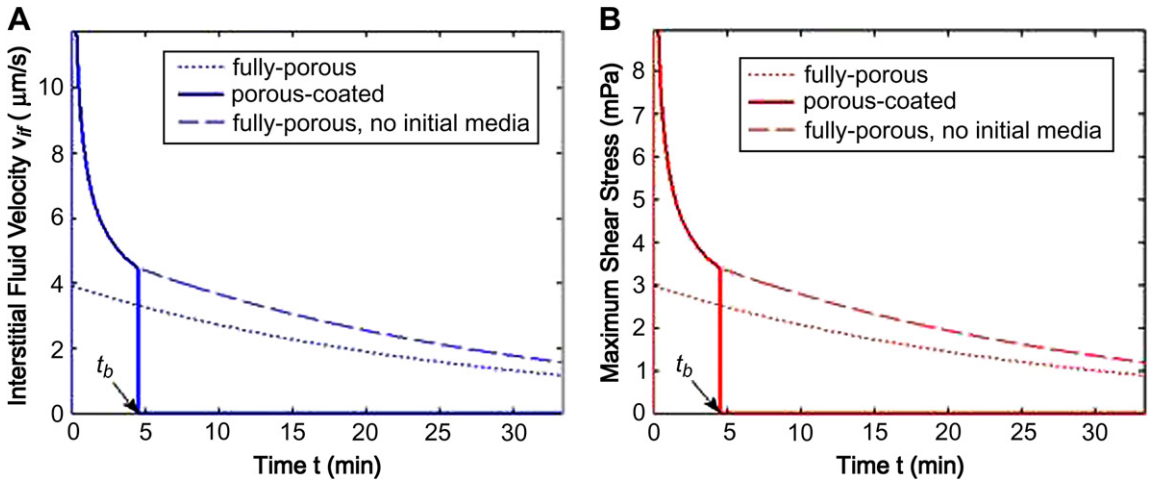

Fig. 3. (A) Interstitial fluid velocity versus time curves for fully porous (dotted), porous-coated (solid) and fully porous no stage 1 (dashed). Cell suspension is added at $t = 0$ for all three cases. Fully porous: exponential decay from $t = 0$ until equilibrium is reached. Note that time constant $\tau = 27.5$ min such that $4\tau = 110$ min yields 98% decay towards the equilibrium condition. Porous-coated: no initial media in porous substrate lead to faster initial velocities, until $t = t_b$ when the fluid reaches the bottom solid disk and velocity drops sharply to zero. Fully porous, no initial media in the culture well: first stage when $t < t_b$ sees fluid flow identical to porous-coated case since there are no initial media. However, fluid is allowed to leak out from the base of the cylinder due to the absence of the solid disk, so fluid levels equilibrate in a similar fashion to the fully porous cylinder, i.e. exponential decay with time constant $\tau = 27.5$ min when $t > t_b$. (B) Shear stress versus time curves for fully porous (dotted), porous-coated (solid) and fully porous no stage 1 (dashed). By scaling arguments, shear stress time profiles are directly proportional to velocity curves. The scaling factor $K = 0.76$ mPa/(μm/s) was determined using computational modeling of flow-through packed spheres.

profiles than cells on porous-coated substrates where media flow-through is restricted. The cells on the porous-coated substrates experienced relatively high initial shear stress followed by an instantaneous drop to zero within the first 5 min of culture. The cells on the fully porous substrate in contrast initially experienced a lower level of shear stress; however, the shear stress profile decays exponentially, and thus much more slowly with respect to time. To support the

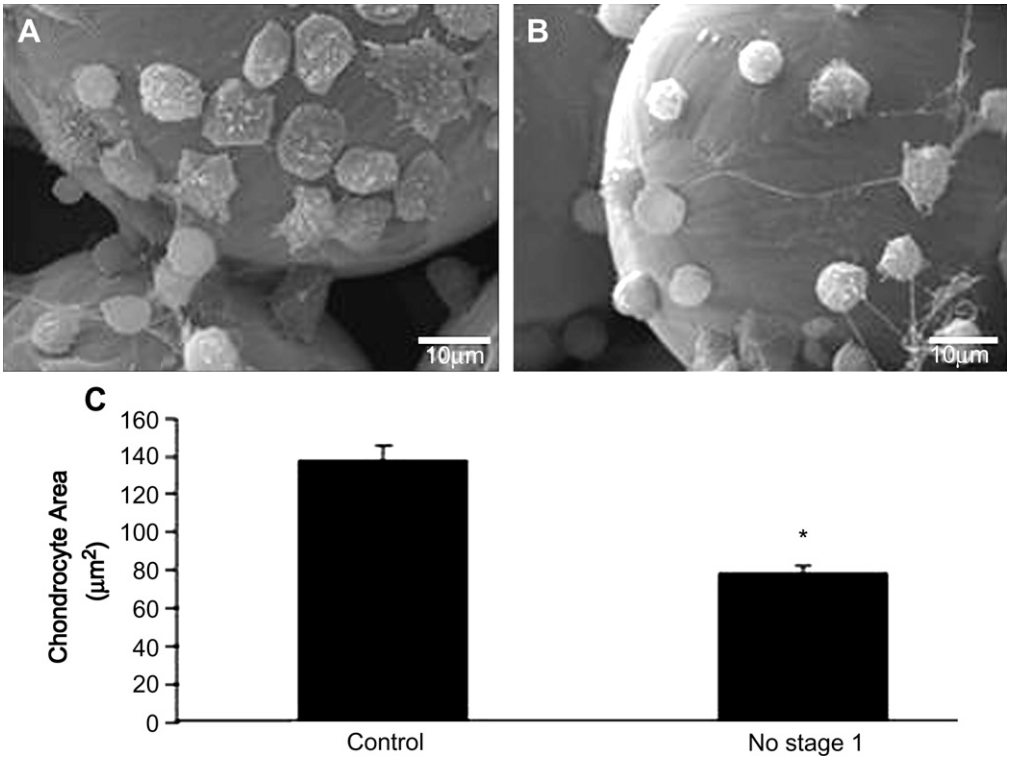

Fig. 4. Chondrocytes grown on the surface of fully porous Ti-6Al-4V substrates in the presence (A) or absence (B) of stage 1 in the seeding protocol. After 24 h in culture, samples were fixed in 2% paraformaldehyde and prepared for examination by scanning electron microscopy. Chondrocytes grown under normal seeding conditions appear to be spread whereas those grown without stage 1 of seeding display a rounded morphology. (C) Chondrocyte areas on fully porous titanium alloy substrate in the presence (Control) and absence of stage 1 (No Stage 1) in the seeding protocol. The cell size was determined by measuring the cell area in scanning electron micrographs as described in Section 2. The results from three experiments were pooled and expressed as the mean ± SEM, $n \geq 100$ cells. $^*p < 0.001$ when compared to respective Control.

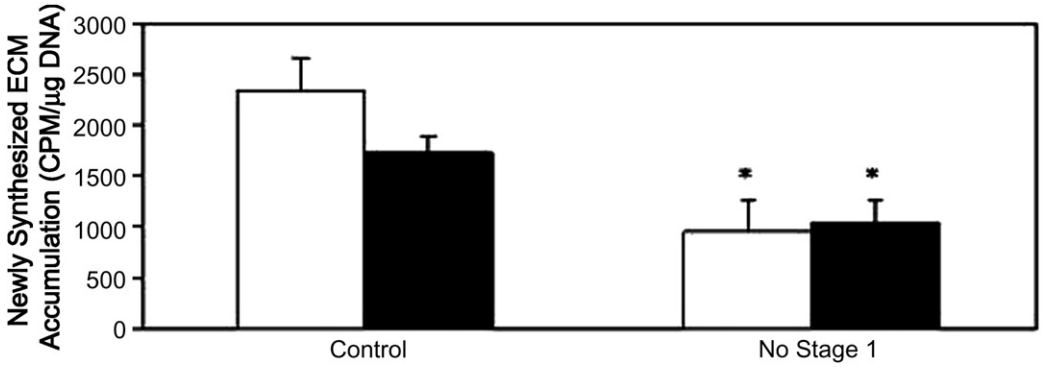

Fig. 5. Newly synthesized proteoglycan (open) and collagen (filled) accumulation by chondrocytes on fully porous titanium alloy substrate grown in the presence (Control) and absence of stage 1 (No Stage 1) in the seeding protocol. Cells were incubated with $[^{35}S]-SO_4$ and $[^{3}H]$-proline to label sulphated proteoglycans and collagens, respectively, immediately following cell seeding. Radioactivity incorporation was quantified as described in Section 2. Accumulation was normalized to DNA. Results from all experiments are pooled and expressed as the mean ± SEM, $n = 9$. $*p < 0.001$ when compared with Control.

hypothesis that these shear stress profiles can influence function, we examined chondrocyte spreading and matrix accumulation (parameters that we had shown previously were altered by substrate architecture) following alteration of the seeding protocol to mimic the effects of the extent of porosity on shear forces. As we were able to reproduce the effects of substrate porosity, this appeared to validate the predictions from our model system. Furthermore we demonstrated that integrins, in particular the α5β1 integrin, were involved in mechanotransduction as blocking integrin binding resulted in cell shape and matrix accumulation that was similar to that seen when cells were placed on porous-coated substrates

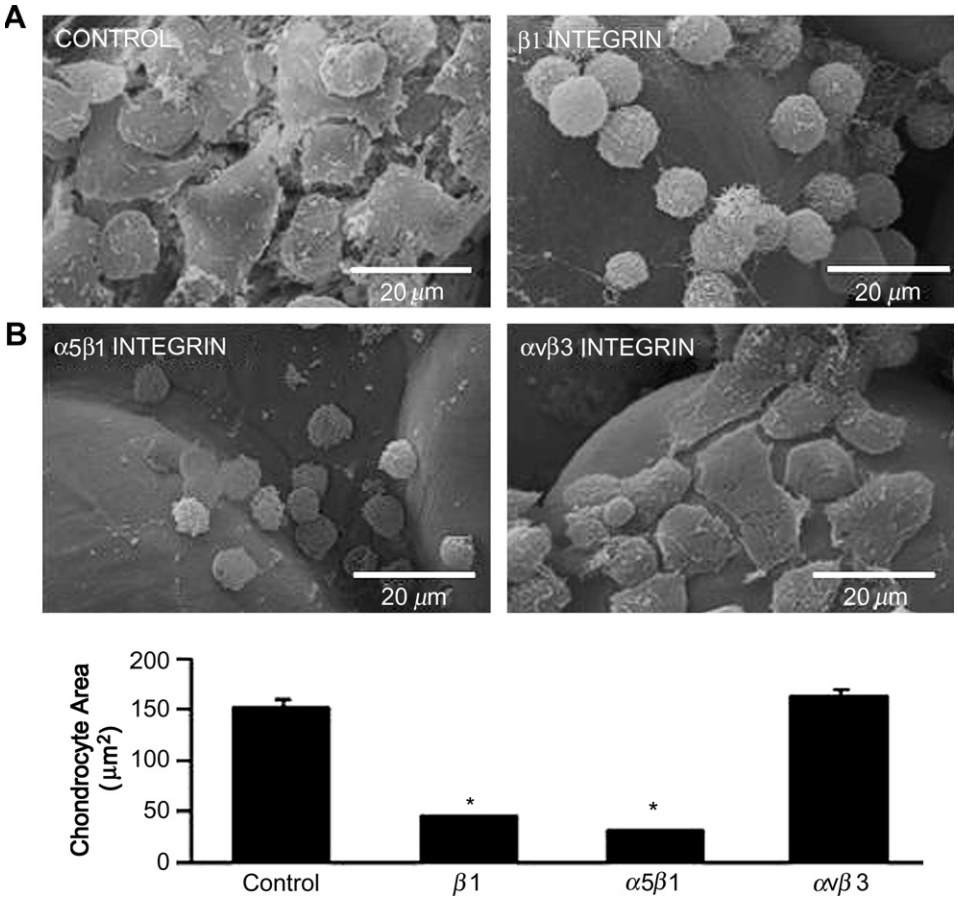

Fig. 6. (A) Chondrocytes grown on the surface of fully porous Ti-6Al-4V substrates in the absence (control, IgG1 isotype) or presence of α1, α5β1 and αvβ3 integrin antibodies for 24 h. Samples were then processed for scanning electron microscopy. Scale bar = 20 μm. (B) Areas of chondrocytes grown on the surface of fully porous Ti-6Al-4V substrates in the presence and absence of α1, α5β1 and αvβ3 integrin antibodies at 24 h. The cell area in the scanning electron micrographs was measured as described in Section 2. The results from three experiments were pooled and expressed as the mean ± SEM, $n \geq 100$ cells. $*p < 0.001$ when compared to Control.

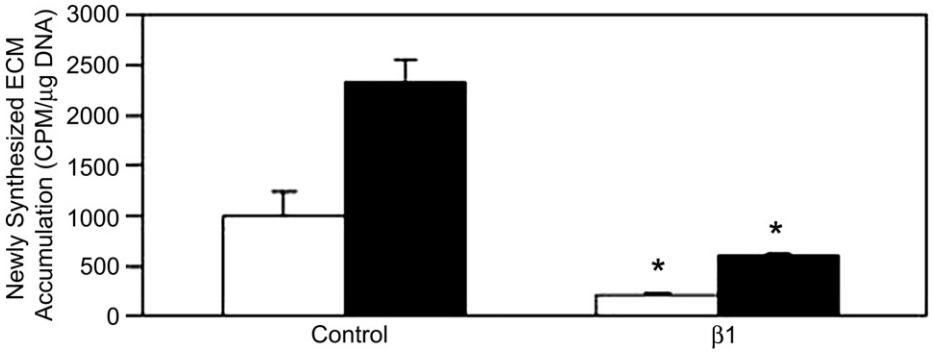

Fig. 7. Amount of newly synthesized extracellular matrix (ECM) accumulated per cell in the presence of the β1 integrin function-blocking antibody or its isotype control (Control) by chondrocytes grown on fully porous Ti-6Al-4V. The cells were incubated with $^{35}S-SO_4$ and ^{3}H proline to label proteoglycan (filled) or collagen (unfilled), respectively. The amount of radioactivity incorporated was normalized for DNA content, pooled and expressed as the mean ± SEM, $n = 9$. $*p < 0.001$ when compared with respective control.

where fluid flow was limited. Furthermore, these findings demonstrate the importance of chondrocyte morphology in affecting extracellular matrix synthesis and ultimately, tissue formation.

The BCC unit cell arrangement of spheres as a model geometry of the porous substrates provided a good baseline for estimating local variations in interstitial fluid velocity and wall shear stress. The unit cell model lent itself to our computational fluid dynamics simulations because its self-repeating nature permitted periodic (symmetric) boundary conditions that considerably reduced computation time. To ensure proper convergence of the numerical solution, two unit cells were vertically stacked to sufficiently distance the downstream outlet boundary from the inlet boundary. The numerical results confirmed that the fluid motion was identical from one unit cell to another, and that an outlet boundary two unit cells away had little effect on the upstream inlet boundary condition, as expected for low Reynolds number laminar flow. Furthermore, the numerical results were consistent with the expectation that cross-sections with the least available area for fluid penetration would have the largest increase in interstitial fluid velocity, and that maximum shear stress would occur near the sphere equator [19]. Although the structural heterogeneity of our experimental samples would result in more non-uniform fluid motion throughout the substrate and higher local velocity and shear stress in specific regions, we expect that our current estimates provide a general sense of the local magnitudes and spatial variations within the system without the need for simulating flow around a more realistic but complex representation of the pore architecture.

Our analysis of shear stress time profiles is based on classical Darcy's law for flow through porous media. Close examination of the derived equations revealed that the largest source of error in our predicted time profiles could be attributed to the cited specific permeability k of the porous substrates. The empiricism of this parameter is notorious for being critically dependent on material and geometric properties. Thus, use of any empirical relationship relating k to porosity ϕ alone must be done cautiously, and applied to systems with strong similarity to the system from which the relationship was first derived. We used a relationship for $k(\phi)$ determined originally for porous titanium by rolling powder, which presumably is much different from porous titanium alloy formed by sintered spherical beads. To our knowledge, specific permeability has not yet been reported for Ti-6Al-4V sintered beads. Our equations suggest that $k(\phi)$ is important in both the initial velocity condition and the time constant of the systems governed by exponential decays. However, since the time constant is indirectly proportional to k, an order of magnitude increase or decrease in k would result in a corresponding change in time constant to $\tau = 3$ min or $\tau = 4.5$ h, respectively. Neither extreme was observed experimentally. Rather, the calculated value of $\tau = 27.5$ min was much more indicative of our experimental observations, supporting the $k(\phi)$ relationship used.

Two major assumptions were made in deriving the time-dependent velocity and stress curves. The first important assumption was that the time-dependent fluid motion in all flow regions was quasi-steady. This assumption allowed us to apply Darcy's law and steady state flow conditions at each instant in time. The quasi-steady assumption is valid for all flows belonging to the Stokes flow regime, where $\mathrm{Re} \ll 1$. In our experiments, $\mathrm{Re} \sim 10^{-4}$ based on characteristic interstitial fluid velocity $v_{if} \sim 10^{-6}$ m/s, pore diameter $a \sim 10^{-4}$ m, fluid density $\rho \sim 10^{3}$ kg/m^3, and dynamic viscosity $\mu \sim 10^{-3}$ kg/ms. Thus, the Stokes flow assumption appears most appropriate for our analysis.

The second and likely more important supposition was that the cell suspension was a continuous phase, and that the cells themselves had negligible effect on the fluid flow and rheological properties of the suspension. This assumption may have been valid in the fluid region outside the tubing and also just above the substrate, where the length scales were relatively large compared to cell size. However, the continuum assumption most likely broke down within the interstices of the porous structure since cells were of the same magnitude in terms of size as the average pore diameter (10 μm cell diameter compared to 75 μm average pore size). Thus, fluid flow was likely influenced by particle–particle and particle–fluid interactions that would require analysis of multiphase hydrodynamics. Such particulate flows are difficult even for the simplest geometries. Analysis of these interactions in

complex, tortuous geometries would be beyond any theoretical treatment, and unfortunately, also beyond the current capabilities of numerical simulation.

Another assumption made was that the shear stress time curves represented stress actually exerted on the cells by the flowing fluid, as if all cells resided on the surface of the beads. In reality, during the early stages of fluid flow, the cells were being carried in suspension through the pores. During this time, tumbling cells may experience physical interactions with other cells and with the titanium beads without necessarily anchoring onto the substrate surface. Therefore, since the shear stress curves were applied only on the bead surfaces, it is difficult to conclude that the predicted curves are truly representative of the stresses experienced by the cells during the entire time period. Nevertheless, using a fully porous substrate without stage 1 seeding indeed combined two separate time profile segments from the other two experiments. Initial percolation of the cell suspension was identical to the porous-coated case since no media was present initially in both cases. Once the fluid reached the bottom of the tubing, the bottom permitted fluid leakage out into the well, which was similar to the fully porous case. Thus, this experiment provided evidence that the time profile segment was more critical to final chondrocyte morphology.

The present study revealed that variations in shear stress profiles occur on the surface of fully porous versus porous-coated substrates. Shear stimulation has been previously shown to significantly enhance both collagen and proteoglycan synthesis in cartilage explants and bioengineered constructs [7–9,21–27]. As well, Smith et al. showed that fluid-induced shear stress applied to articular chondrocytes at an amplitude of as low as 1.6 Pa altered both the morphology and the metabolism of adult human and bovine articular chondrocytes [7]. This level of shear stress resulted in a 2-fold increase in glycosaminoglycan synthesis and induced changes in chondrocyte shape from a round to a more elongated and elliptical morphology [7]. The maximum shear stress calculated on the substrates in the current study was estimated to be between 3 and 9 mPa. While few studies have focused on characterizing the hydrodynamic environment by modeling the flow profile and quantifying the associated fluid velocities and hydrodynamic forces, the shear stresses calculated in the current system appear to be quite low. However, Bilgen et al. demonstrated that low-shear hydrodynamic forces could enhance extracellular matrix deposition by articular chondrocytes [10]. These shear stresses, in the range of 0–60 mPa were shown to enhance chondrocyte proliferation and matrix synthesis.

The mechanisms by which chondrocytes are able to sense changes in their mechanical environment and respond by altering their morphology and production of matrix proteins are largely unknown. Some authors believe that it is the change in chondrocyte morphology that dictates cell metabolism, rather than the mechanical environment itself. Millward-Sadler and Salter have documented that by maintaining chondrocyte morphology, pressure-induced changes in biochemical and molecular responses are inhibited [11]. In order to recognize mechanical stimuli, chondrocytes must express cell membrane mechanoreceptors that transduce these mechanical signals intracellularly, resulting in changes in cell morphology. Integrins have been implicated as mechanotransducers involved in the early cellular response to mechanical stimulation [11–14,28,29]. Application of shear forces has been previously shown to enhance the binding of various integrins to their specific ligands [11]. Following binding to their extracellular matrix ligands, integrins have been shown to cluster, thereby promoting their association with the actin cytoskeleton, ultimately leading to the formation of stress fibres and resulting in changes in chondrocyte morphology [11]. It is this remodelling of the actin cytoskeleton and associated changes in cell shape that are believed to result in changes in matrix synthesis. In the current study, chondrocyte spreading was inhibited by blocking integrin binding through the use of function-specific integrin antibodies. This inhibition led to a corresponding decrease in matrix synthesis, thereby suggesting a role for chondrocyte spreading in regulating cell biosynthesis. It is traditionally believed that a flattened chondrocyte morphology is associated with dedifferentiation of the cell to a more fibroblastic phenotype [30]. In contrast to this flattened morphology, the spread chondrocytes in this study exhibit a more polygonal shape. This suggests that there may be an optimal, intermediate degree of cell spreading for chondrocytes that favours cartilage tissue formation and this should be taken into consideration when designing substrates.

Aside from fluid-induced shear stresses, other factors may be contributing to the effects of substrate geometry on chondrocyte spreading and matrix accumulation *in vitro*. Such mechanisms may include nutrient and waste transport through the various substrates. As previously reported, chondrocytes in culture require sufficient nutrient transfer from the culture medium and must be free to remove waste by-products from their vicinity [31]. Chondrocytes *in vivo* undergo predominantly anaerobic respiration due to the avascular nature of cartilage. This results in high levels of lactic acid production that must be exported from the cell for intracellular pH to be maintained [32]. Furthermore, an adequate supply of oxygen is required for articular chondrocytes to sustain their predominantly glycolytic respiration. As glucose is also a precursor for proteoglycan synthesis, limited availability of this molecule could hinder proteoglycan synthesis [33]. While possible, these mechanisms appear unlikely, as cell densities in this study are relatively low, thus nutrient and waste transport should not be limited. Furthermore, preliminary studies have shown that addition of sodium bicarbonate, which was used to buffer acidity in our system, did not affect the results (data not shown).

5. Conclusions

The shear stress time profiles experienced by cells on the surface of fully porous substrates were shown to differ from those on porous-coated substrates, and these forces likely influenced chondrocyte spreading, and extracellular matrix

accumulation. Chondrocytes were able to sense changes in their hydrodynamic environments resulting from the different substrate architectures, via α5β1 integrins. This study indicates the importance of characterizing spatial and temporal shear stresses applied to chondrocytes when designing substrates for cartilage tissue engineering. Characterization of the mechanical and molecular mechanisms involved in regulating cartilage tissue formation may ultimately lead to the optimization of *in vitro* cartilage formation methods for clinically relevant tissue production.

Acknowledgements

Supported by the Canadian Institutes of Health Research, Natural Sciences and Engineering Research Council (NSERC) of Canada, and the Arthritis Society of Canada. Caroline Spiteri is a recipient of the NSERC Canada Graduate Scholarship. The authors would also like to acknowledge Mr. H. Bojarski and Ryding-Regency Meat Packers for providing the tissues, Marie Maguire for secretarial support, and Dr. Jason Hong for fabricating the titanium alloy substrates.

Appendix

We derive relationships for interstitial fluid velocities through fully porous and porous-coated substrates from the time the cell suspension is first added until the system reaches equilibrium (referred to as stage 2 in the main text). Doing so allows us to estimate timescales involved for sedimentation, attachment, and exposure to shear forces of the cells introduced into the different systems. Note that the derivations are carried out for superficial velocities, but it is trivial to convert these to interstitial fluid velocities.

Fig. A1 illustrates the fully porous substrate system, consisting of a porous circular disk of thickness L and porosity ϕ, contained within cylindrical tubing of inner radius r_{it} and outer radius r_{ot}, all centred in a circular well of inner radius r_{iw}. The fluid interface levels z_i and z_o for inside and outside the tubing, respectively, adjust themselves in the vertical z-direction under the combined effect of hydrostatic and surface tension forces until they reach an equilibrium height. Before addition of the cell suspension, the interface levels are separated by an equilibrium height difference $h_0 = z_i(t = 0^-) - z_o$ governed by:

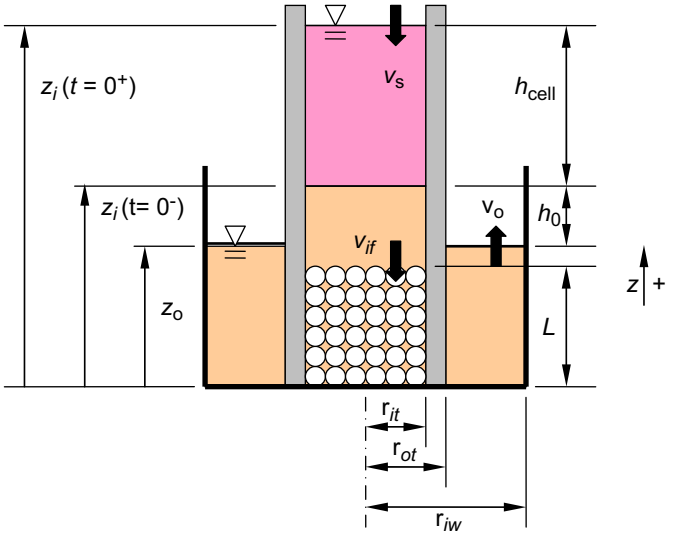

Fig. A1. Diagram of fully porous substrate system at $t = 0$ when cell suspension is added into the tubing

$$h_0 = \frac{2\gamma\cos\theta}{\rho g r_{it}} \tag{1}$$

where ρ is the fluid density, g is acceleration due to gravity, and γ and θ are the surface tension and contact angle, respectively, of the solid–liquid interface inside the tubing. h_0 is typically called the capillary height. After the addition of the cell suspension, the new height difference $h = z_i(t = 0^+) - z_o$ becomes the sum of the capillary height and the height of the added cell suspension column, h_{cell}. This increases the hydrostatic pressure inside the tubing, and drives fluid from within the tubing out into the well via the porous substrate.

As illustrated in Fig. A1, fluid velocities are distinct in three separate regions of the system. v_s is the velocity in the fluid column resting above the porous substrate, and is traditionally referred to as the superficial velocity. v_{if} is the velocity of the fluid within the interstices of the substrate. Finally, v_o is the outflow velocity of fluid in the well outside the tubing. For our purposes, we assume that these velocities apply uniformly throughout their respective sections. From conservation of mass, we can relate the three velocities by:

$$v_s \pi r_{it}^2 = v_{if}\phi\pi r_{it}^2 = v_o \pi\left(r_{iw}^2 - r_{ot}^2\right) \tag{2}$$

where we have assumed the directions shown in the figure, and assigned positive values to the velocities. It can be easily shown that

$$v_s = -\frac{dz_i}{dt}, \tag{3}$$

$$v_o = \frac{dz_o}{dt}, \tag{4}$$

$$\frac{dh}{dt} = \frac{dz_i}{dt} - \frac{dz_o}{dt} \tag{5}$$

where $h = z_i - z_o$ is the time-dependent height difference between interfaces. Substituting Eqs. (3)–(5) into Eq. (2) and rearranging yields:

$$-\frac{dz_i}{dt}\pi r_{it}^2 = \left(\frac{dz_i}{dt} - \frac{dh}{dt}\right)\pi\left(r_{iw}^2 - r_{ot}^2\right)$$

$$\frac{dh}{dt} = \frac{dz_i}{dt}\left(\frac{r_{iw}^2 - r_{ot}^2 + r_{it}^2}{r_{iw}^2 - r_{ot}^2}\right) = -v_s\left(\frac{r_{iw}^2 - r_{ot}^2 + r_{it}^2}{r_{iw}^2 - r_{ot}^2}\right) \tag{6}$$

Next, using Darcy's law for flow through a porous medium [34], the superficial velocity can be related to the system properties by:

$$v_s = \frac{k}{\mu}\frac{\Delta p}{L} = \frac{k}{\mu}\frac{\rho g(h-h_0)}{L} \tag{7}$$

In Eq. (7), k is the specific permeability of the porous substrate, in units of [m^2], μ is the fluid dynamic viscosity, and Δp is the pressure drop across the porous bed, equal to the hydrostatic pressure created by the height difference between interface levels. Care is taken to account for the capillary height h_0, which itself does not contribute to the driving force that pushes the fluid through the porous bed. Differentiating Eq. (7) then yields:

$$\frac{dv_s}{dt} = \frac{k\rho g}{\mu L}\left(\frac{dh}{dt} - \frac{dh_0}{dt}\right) = \frac{k\rho g}{\mu L}\frac{dh}{dt} \tag{8}$$

since h_0 is constant. Finally, substituting Eq. (8) into Eq. (6) gives a first-order differential equation in v_s, as follows:

$$\frac{dv_s}{dt} = -\frac{k\rho g}{\mu L}\left(\frac{r_{iw}^2 - r_{ot}^2 + r_{it}^2}{r_{iw}^2 - r_{ot}^2}\right)v_s \tag{9}$$

The solution to Eq. (9) is easily found to be in the form of an exponential decay:

$$v_s(t) = v_{init}e^{-t/\tau} \tag{10}$$

where v_{init} is the initial superficial velocity:

$$v_{init} = \frac{k\rho g}{\mu L}h_{cell} \tag{11}$$

and τ is the time constant of the system, given by:

$$\tau = -\frac{\mu L}{k\rho g}\left(\frac{r_{iw}^2 - r_{ot}^2}{r_{iw}^2 - r_{ot}^2 + r_{it}^2}\right) \tag{12}$$

Interstitial fluid velocity is then easily obtained from superficial velocity by Eq. (2).

Fig. A2 illustrates the porous-coated substrate system. The porous substrate of thickness L and porosity ϕ rests on a solid disk of thickness T that prevents fluid from flowing into the well from the tubing, and vice versa. Similar to the fully porous substrate, the substrate is encased in tubing of inner radius r_{it} and outer radius r_{ot}, and centred in a well of inner radius r_{iw}. In contrast to the conditions of the fully porous case, however, there is initially no fluid inside and outside the tubing. Thus, at $t = 0$ when the cell suspension is added, the entire fluid column of height h_{cell} rests on the top surface of the porous-coated substrate (see Fig. A2A), and fluid is allowed to immediately flow into the pores due to gravity. The fluid penetrates into the porous bed and eventually reaches the bottom of the bed (or top of the solid disk) at $t = t_b$, when all fluid motion ceases, i.e. for all $t > t_b$, $v_s = v_{if} = 0$.

During the period $0 < t < t_b$ when the fluid is percolating through the porous bed, the upper and lower interfaces of the fluid column move vertically downward at different velocities (see Fig. A2B). The upper interface at position z_u moves at a superficial velocity v_s, while the lower interface at position z_l moves at interstitial fluid velocity v_{if}. As the lower interface moves during the period $0 < t < t_b$, the fluid penetration depth s increases from $0 < s < L$ while the interface height difference h increases from $h_{cell} < h < h_b$, where h_b is the height of fluid for $t > t_b$.

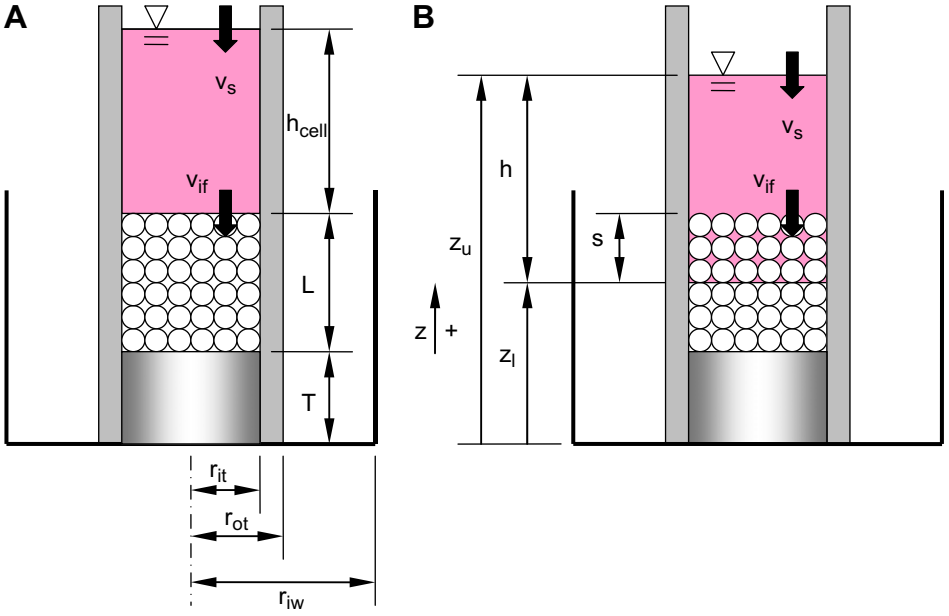

Fig. A2. Diagram of porous-coated substrate system at (A) $t = 0$ when cell suspension is added to the tubing, and (B) at a later time t when the fluid has entered the pores of the substrate.

Considering the definitions above, we have the following geometric and kinematic relationships:

$$h = h_{\text{cell}} + (1-\phi)s \tag{13}$$

$$v_{\text{s}} = v_{\text{if}}\phi \tag{14}$$

$$v_{\text{s}} = -\frac{\mathrm{d}z_{\text{u}}}{\mathrm{d}t} \tag{15}$$

$$v_{\text{if}} = -\frac{\mathrm{d}z_{\text{l}}}{\mathrm{d}t} \tag{16}$$

$$\frac{\mathrm{d}h}{\mathrm{d}t} = \frac{\mathrm{d}z_{\text{u}}}{\mathrm{d}t} - \frac{\mathrm{d}z_{\text{l}}}{\mathrm{d}t} = -v_{\text{s}} + v_{\text{if}} = v_{\text{s}}\left(\frac{1-\phi}{\phi}\right) \tag{17}$$

Similar to the fully porous case, the superficial velocity can be determined by Darcy's Law, with the main difference in this case being that the porous bed depth is not constant L, but is instead the variable fluid penetration depth s. Eq. (7) above must therefore be modified to read:

$$v_{\text{s}} = \frac{k}{\mu}\frac{\rho g(h-h_0)}{s} \tag{18}$$

Using Eq. (13) to eliminate s in favour of h, we have:

$$v_{\text{s}}(h) = \frac{k\rho g(1-\phi)}{\mu}\frac{(h-h_0)}{(h-h_{\text{cell}})} \tag{19}$$

which gives v_{s} as a function of h only. Next, we substitute Eq. (17) to obtain:

$$\frac{\mathrm{d}h}{\mathrm{d}t} = \frac{k\rho g(1-\phi)^2}{\mu\phi}\frac{(h-h_0)}{(h-h_{\text{cell}})} \tag{20}$$

This is a first-order non-linear differential equation that can be solved using separation of variables to yield:

$$(h-h_0) + (h_0-h_{\text{cell}})\ln(h-h_0) = \frac{k\rho g(1-\phi)^2}{\mu\phi}t + C_0 \tag{21}$$

where C_0 is a constant of integration. Using the initial condition that $h = h_{\text{cell}}$ at $t = 0$, C_0 is found to be:

$$C_0 = (h_{\text{cell}}-h_0) + (h_0-h_{\text{cell}})\ln(h_{\text{cell}}-h_0) \tag{22}$$

Eq. (21) can then be simplified to:

$$t(h) = \frac{\mu\phi}{k\rho g(1-\phi)^2}\left[(h-h_{\text{cell}}) + (h_0-h_{\text{cell}})\ln\left(\frac{h-h_0}{h_{\text{cell}}-h_0}\right)\right] \tag{23}$$

Eqs. (19) and (23) completely determine v_{s} as a function of time t. Unfortunately, the inversion of the function $t(h)$ to $h(t)$ is non-trivial, and leads to use of the Lambert W function, so a closed form solution of $v_{\text{s}}(t)$ becomes cumbersome. For practical reasons, we leave the solution in the form of Eqs. (19) and (23), and recognize that $v_{\text{s}}(t)$ can be easily obtained by first calculating both $v_{\text{s}}(h)$ and $t(h)$ for the range $h_{\text{cell}} < h < h_{\text{b}}$, and then relating v_{s} to t directly.

References

[1] Spiteri CG, Pilliar RM, Kandel RA. Substrate porosity enhances chondrocyte attachment, spreading, cartilage tissue formation *in vitro*. J Biomed Mater Res A 2006;78:676–83.

[2] Loeser RF. Integrins and cell signaling in chondrocytes. Biorheology 2002;39:119–24.

[3] Knudson W, Loeser RF. CD44 and integrin matrix receptors participate in cartilage homeostasis. Cell Mol Life Sci 2002;59:36–44.

[4] Hynes RO. Integrins: bidirectional, allosteric signaling machines. Cell 2002;110:673–87.

[5] Pulai JI, Del Jr CM, Loeser RF. The alpha5beta1 integrin provides matrix survival signals for normal and osteoarthritic human articular chondrocytes *in vitro*. Arthritis Rheum 2002;46:1528–35.

[6] Ciolfi VJ, Pilliar R, McCulloch C, Wang SX, Grynpas MD, Kandel RA. Chondrocyte interactions with porous titanium alloy and calcium polyphosphate substrates. Biomaterials 2003;24:4761–70.

[7] Smith RL, Donlon BS, Gupta MK, Mohtai M, Das P, Carter DR, et al. Effects of fluid-induced shear on articular chondrocyte morphology and metabolism *in vitro*. J Orthop Res 1995;13:824–31.

[8] Smith RL, Carter DR, Schurman DJ. Pressure and shear differentially alter human articular chondrocyte metabolism: a review. Clin Orthop Relat Res 2004:S89–95.

[9] Waldman SD, Spiteri CG, Grynpas MD, Pilliar RM, Kandel RA. Long-term intermittent shear deformation improves the quality of cartilaginous tissue formed *in vitro*. J Orthop Res 2003;21:590–6.

[10] Bilgen B, Sucosky P, Neitzel GP, Barabino GA. Flow characterization of a wavy-walled bioreactor for cartilage tissue engineering. Biotechnol Bioeng 2006;95:1009–22.

[11] Millward-Sadler SJ, Salter DM. Integrin-dependent signal cascades in chondrocyte mechanotransduction. Ann Biomed Eng 2004;32:435–46.

[12] Millward-Sadler SJ, Wright MO, Davies LW, Nuki G, Salter DM. Mechanotransduction via integrins and interleukin-4 results in altered aggrecan and matrix metalloproteinase 3 gene expression in normal, but not osteoarthritic, human articular chondrocytes. Arthritis Rheum 2000;43:2091–9.

[13] Mobasheri A, Carter SD, Martin-Vasallo P, Shakibaei M. Integrins and stretch activated ion channels; putative components of functional cell surface mechanoreceptors in articular chondrocytes. Cell Biol Int 2002;26:1–18.

[14] Orazizadeh M, Cartlidge C, Wright MO, Millward-Sadler SJ, Nieman J, Halliday BP, et al. Mechanical responses and integrin associated protein expression by human ankle chondrocytes. Biorheology 2006;43:249–58.

[15] Bhardwaj T, Pilliar RM, Grynpas MD, Kandel RA. Effect of material geometry on cartilagenous tissue formation *in vitro*. J Biomed Mater Res 2001;57:190–9.

[16] Boyle J, Luan B, Cruz TF, Kandel RA. Characterization of proteoglycan accumulation during formation of cartilagenous tissue *in vitro*. Osteoarthr Cartil 1995;3:117–25.

[17] Wang H, Kandel RA. Chondrocytes attach to hyaline or calcified cartilage and bone. Osteoarthr Cartil 2004;12:56–64.

[18] Kim YJ, Sah RL, Doong JY, Grodzinsky AJ. Fluorometric assay of DNA in cartilage explants using Hoechst 33258. Anal Biochem 1988;174:168–76.

[19] White F. Fluid mechanics. 5th ed. New York: McGraw-Hill; 2003.

[20] Tikhonov GF, Sorokin VK. Preparation of porous titanium by rolling powder. Powder Metall Met Ceram 1969;8:167–9.

[21] Bueno EM, Bilgen B, Barabino GA. Wavy-walled bioreactor supports increased cell proliferation and matrix deposition in engineered cartilage constructs. Tissue Eng 2005;11:1699–709.

[22] Davisson T, Sah RL, Ratcliffe A. Perfusion increases cell content and matrix synthesis in chondrocyte three-dimensional cultures. Tissue Eng 2002;8:807–16.

[23] Gemmiti CV, Guldberg RE. Fluid flow increases type II collagen deposition and tensile mechanical properties in bioreactor-grown tissue-engineered cartilage. Tissue Eng 2006;12:469–79.

[24] Jin M, Frank EH, Quinn TM, Hunziker EB, Grodzinsky AJ. Tissue shear deformation stimulates proteoglycan and protein biosynthesis in bovine cartilage explants. Arch Biochem Biophys 2001;395:41–8.

[25] Jin M, Emkey GR, Siparsky P, Trippel SB, Grodzinsky AJ. Combined effects of dynamic tissue shear deformation and insulin-like growth factor I on chondrocyte biosynthesis in cartilage explants. Arch Biochem Biophys 2003;414:223–31.

[26] Raimondi MT, Moretti M, Cioffi M, Giordano C, Boschetti F, Lagana K, et al. The effect of hydrodynamic shear on 3D engineered chondrocyte systems subject to direct perfusion. Biorheology 2006;43:215–22.

[27] Waldman SD, Spiteri CG, Grynpas MD, Pilliar RM, Hong J, Kandel RA. Effect of biomechanical conditioning on cartilaginous tissue formation *in vitro*. J Bone Joint Surg Am 2003;85-A(Suppl. 2):101–5.

[28] Lee HS, Millward-Sadler SJ, Wright MO, Nuki G, Salter DM. Integrin and mechanosensitive ion channel-dependent tyrosine phosphorylation of focal adhesion proteins and beta-catenin in human articular chondrocytes after mechanical stimulation. J Bone Miner Res 2000;15:1501–9.

[29] Millward-Sadler SJ, Wright MO, Lee H, Caldwell H, Nuki G, Salter DM. Altered electrophysiological responses to mechanical stimulation and abnormal signalling through alpha5beta1 integrin in chondrocytes from osteoarthritic cartilage. Osteoarthr Cartil 2000;8:272–8.

[30] Lee SJ, Lee YM, Han CW, Lee HB, Khang G. Response of human chondrocytes on polymer surfaces with different micropore sizes for tissue-engineered cartilage. J Appl Polym Sci 2004;92:2784–90.

[31] Vunjak-Novakovic G, Obradovic B, Martin I, Bursac PM, Langer R, Freed LE. Dynamic cell seeding of polymer scaffolds for cartilage tissue engineering. Biotechnol Prog 1998;14:193–202.

[32] Meredith D, Bell P, McClure B, Wilkins R. Functional and molecular characterisation of lactic acid transport in bovine articular chondrocytes. Cell Physiol Biochem 2002;12:227–34.

[33] Windhaber RA, Wilkins RJ, Meredith D. Functional characterisation of glucose transport in bovine articular chondrocytes. Pflugers Arch 2003;446:572–7.

[34] Scheidegger AE. The physics of flow through porous media. Toronto, Canada: University of Toronto Press; 2007. p. 73–151.